Appl Nanosci (2015) 5:419–424
DOI 10.1007/s13204-014-0333-2

ORIGINAL ARTICLE

Comparative study of carbon dioxide sensing by Sn-doped TiO_2 nanoparticles synthesized by microwave-assisted and solid-state diffusion route

K. R. Nemade · S. A. Waghuley

Received: 6 May 2014 / Accepted: 18 June 2014 / Published online: 6 July 2014

Abstract Gas sensor based on Sn-doped titanium dioxide (TiO_2) nanoparticles has been fabricated and evaluated for carbon dioxide (CO_2) sensing. The Sn-doped TiO_2 nanoparticles were synthesized by microwave-assisted and solid-state diffusion route. The structure and morphology of resulting samples were characterized by X-ray diffraction (XRD) and scanning electron microscopy (SEM). Ultraviolet–visible (UV–VIS) spectroscopy was employed to study the optical properties. The weight loss of samples was analyzed through thermo gravimetric analysis (TGA). The Sn-doped TiO_2 nanoparticles synthesized through microwave route exhibited good sensing characteristics.

Keywords Carbon dioxide · Microwave assisted · Solid-state diffusion

Introduction

Titanium dioxide (TiO_2) is a potent candidate material for the various modern applications due to its low cost, high chemical inertness, powerful oxidation potential and non-toxicity in water (Choi et al. 2012). TiO_2 is mainly attractive for their notable ability to change the electrical resistance in response to oxidizing and reducing gases (Radecka et al. 2010).

K. R. Nemade (✉)
Department of Applied Physics, J D College of Engineering and Management, Nagpur 441 501, India
e-mail: krnemade@gmail.com

S. A. Waghuley
Department of Physics, Sant Gadge Baba Amravati University, Amravati 444 602, India

In the last two decades, microwave synthesis has arisen as a novel synthesis strategy and method with many significant advances in practical aspects of chemistry (Surati et al. 2012). Lopez et al. (2013) reported the microwave-assisted synthesis of CdS nanoparticles and studied their size evolution. In this study, they reported that the microwave heating has uniform heating characteristics whereas in conventional heating thermal gradient is present.

Sui et al. (2010) reported the synthesis of Sn-doped TiO_2 by sol–gel synthesis with high aspect ratios. Duan et al. (2012) studied the photoanode performance of Sn-doped TiO_2 synthesized by the hydrothermal method. Sn-incorporated rutile TiO_2 nanorods synthesized by simple solvothermal route for photoelectrochemical water splitting have been reported by (Sun et al. 2013). Xiufeng et al. (2011) demonstrated the Sn-doped TiO_2 nanoparticles as a visible-light photocatalyst synthesized by vapor transport method. Radecka et al. (2010) demonstrated the flame spray synthesis route to grow TiO_2-based nanoparticles from which TiO_2:Cr nanosensors were obtained. Al-Homoudi et al. (2007) develop the TiO_2-based CO gas sensor. Resistive response of anatase TiO_2 films is discussed for different concentrations of CO gas.

Wu et al. (2012) studied the ethanol sensing characteristics of Sn-doped rutile TiO_2 nanowires synthesized by a thermal reactive evaporation route. The sensing response increased with an increase in the ethanol concentration. Benkara et al. reported the synthesis of Sn-doped ZnO/TiO_2 by two methods, first is anodic oxidation of Ti foil and another is hydrothermal process. These nanocomposites have been employed as hydrogen gas sensing materials. Chemisorption model was used to explain the H_2 sensing mechanism (Benkara et al. 2013). Nanostructured Sn-doped TiO_2 has been reported by (Raji et al. 2011), which is prepared by ball milling using SnO_2 and TiO_2 as

raw materials. This work pointed out that Sn-doped TiO_2 possessed the highest humidity sensitivity, than pristine TiO_2 and SnO_2.

However, to the best of our knowledge, such kind of comparative study is still not reported in the literature of materials science. So, in the present work, we are studying the comparative sensing response of Sn-doped TiO_2 synthesized by microwave-assisted and solid-state diffusion route towards the carbon dioxide (CO_2). CO_2 is the primary greenhouse gas emitted through human activities, which is responsible for climate change. Therefore, its detection becomes crucial for human being.

The synthesized materials by both routes were characterized through X-ray diffraction (XRD), scanning electron microscope (SEM), ultraviolet–visible spectroscopy (UV–VIS) and thermo gravimetric analysis (TGA). The various gas sensing characteristics were also analyzed comparatively for both route of synthesis.

Experimental

Microwave-assisted synthesis of Sn-doped TiO_2 nanoparticles

The laboratory grade microwave synthesizer CEM Phoenix was used for synthesis of Sn-doped TiO_2 nanoparticles. The starting chemicals, $SnCl_4$ and TiO_2 of AR grade were used in this work. The 0.1 wt % $SnCl_4$ was added in TiO_2 in aqueous media. These solutions were mixed under constant magnetic stirring for 1 h. The mixture was heated in CEM supplied single use vessel. The mixture containing vessel was reacted in the CEM microwave at a temperature of 600 °C.

Synthesis of Sn-doped TiO_2 nanoparticles by solid-state diffusion routes

Sn-doped TiO_2 nanoparticles were prepared by the solid-state diffusion routes using the starting chemicals, $SnCl_4$ and TiO_2. The preparatory materials were mixed thoroughly by taking 0.1 wt % $SnCl_4$ in TiO_2 using the agate mortar pestle for 1 h. The crushed samples were placed in crucible and heated at 973 K in muffle furnace for 8 h. Then, allow to cool down, crushed in the mortar pestle again and heated at 1,173 K for 8 h. Lastly, the samples in the furnace were kept to cool down to room temperature.

Materials characterizations

X-ray diffraction patterns were recorded on Rigaku (Miniflex II) diffractometer with CuKα radiation in the range 10°–70°. The topography of samples was analyzed through SEM using JEOL JSM-7500F. The UV–VIS analysis was performed on Perkin Elmer UV spectrophotometer in the range 375–525 nm. The thermo gravimetric analysis (TGA) was obtained in a Shimadzu DTG-60 h thermal analyzer.

Sensors fabrication and gas sensing measurements

Fabrication of sensors was done through screen printing on chemically cleaned glass SiO_2 substrate of dimension 25 × 25 mm by screen printing technique using a temporary binder. In this way, sensing material deposited SiO_2 substrate kept for heating at 373 K for 1 h. During this stage, volatile organic compounds in binder were evaporated. After this step, highly conducting silver paint was deposited on both side of film to measure change in resistance during the exposure of gas. The voltage divider method was employed to measure the change in resistance. The temperature and pressure inside the sensing chamber were maintained precisely. To measure sensing response, air is used as background gas. The required concentration inside the chamber was maintained by injecting known volume of gas (Nemade and Waghuley 2013). The sensing response of chemiresistor was defined as (Nemade and Waghuley 2014):

$$S = \frac{\Delta R}{R_a} = \frac{|R_g - R_a|}{R_a} \quad (1)$$

where R_a and R_g is the resistance of chemiresistor in air and gas, respectively.

Results and discussion

Figure 1a–c depicts the XRD patterns of the pure TiO_2 and Sn-doped TiO_2 synthesized by microwave-assisted and solid-state diffusion route. The XRD data for both samples were acquired at room temperature (298 K). All diffraction peaks of pure TiO_2 (Fig. 1a) can be indexed to the anatase phase (JCPDS No. 01-070-7348). The average crystallite size was determined with Scherrer equation, $D = K\lambda/\beta\text{Cos}\theta$, where D is average crystallite size, K is shape factor ($K = 0.89$), λ is wavelength of X-ray used for analysis ($\lambda = 1.54$ Å). From the significant and characteristics peaks, the average crystallite size was found to be 18 nm for TiO_2 and 16.7 nm for Sn-doped TiO_2 samples. From XRD patterns, it is noticeable that particle size was not greatly influenced by synthesis route. The exact 2θ position and marginal difference in intensity reflect the good crystallinity of as-synthesized samples. The appearance of diffraction peaks in XRD pattern of Sn-doped TiO_2 at 27 and 34° was assigned to Sn incorporation. The larger effective radius of Sn^{4+} is 0.69 Å compared to that of Ti^{4+}

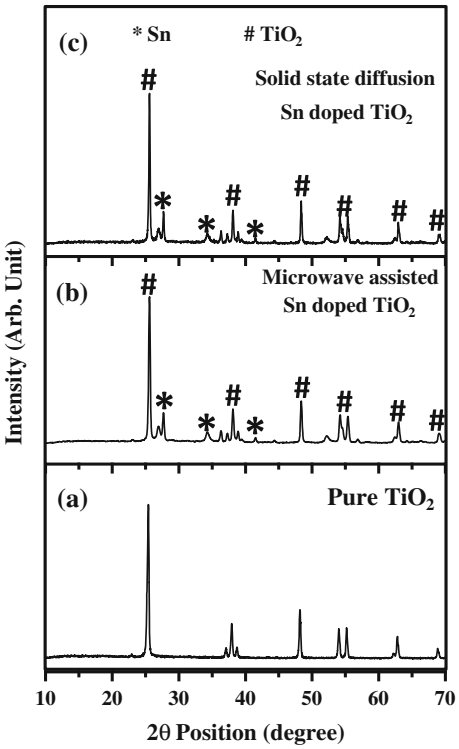

Fig. 1 XRD patterns for (**a**) pure TiO_2 and Sn-doped TiO_2 nanoparticles synthesized by (**b**) microwave-assisted and (**c**) solid-state diffusion route

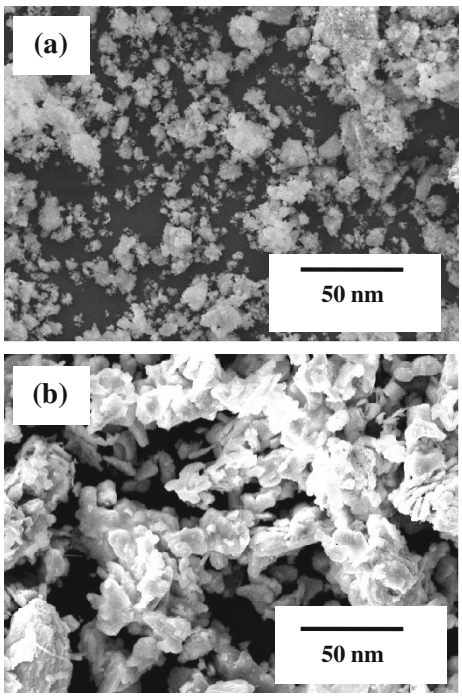

Fig. 2 SEM image of Sn-doped TiO_2 nanoparticles synthesized by (**a**) microwave-assisted and (**b**) solid-state diffusion route

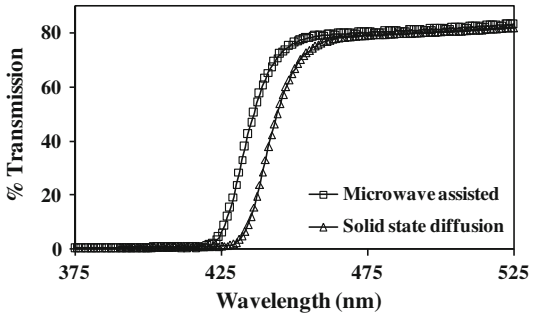

Fig. 3 UV–VIS spectrum of Sn-doped TiO_2 nanoparticles synthesized by microwave-assisted and solid-state diffusion route

that is 0.61 Å, which results in appearance of peaks (Duan et al. 2012).

To determine the morphology of Sn-doped TiO_2 samples, powder of the sample was suspended in acetone under sonication for 30 min. Figure 2a, b shows the SEM of Sn-doped TiO_2 synthesized by microwave-assisted and solid-state diffusion route. As can be seen from micrograph, nanoparticles take the shape like flakes of random size. From micrograph, it is observed that flakes of Sn-doped TiO_2 synthesized by microwave-assisted route are more separate than those synthesized by solid-state diffusion route.

Figure 3 shows the UV–VIS spectra of Sn-doped TiO_2 nanoparticles synthesized by microwave-assisted and solid-state diffusion route. The result shows that the absorption value of Sn-doped TiO_2 nanoparticle synthesized through microwave-assisted route shifts towards lower wavelength. According to effective mass approximation, particle size and band gap are inversely related to each other (Nemade and Waghuley 2014). Similarly, absorption of wavelength by particle is a function of particle size. Therefore, shift towards the lower wavelength results in the increase of band gap. This also shows the reduced number of defects on particle surface. Therefore, microwave-assisted synthesized nanoparticles have large band gap than nanoparticles synthesized through solid-state diffusion route. This change in band gap was related with various optical properties, such as optical conductivity, extinction coefficient and optical dielectric constant.

Figure 4 shows the TGA plot for the as-synthesized Sn-doped TiO_2 nanoparticles. TGA curve clearly shows that synthesized sample continuously lost its weight over the temperature range from room temperature to 725 K. TGA curves for both the samples do not show endothermic or exothermic peaks. This shows that during heating treatment nanoparticles do not undergo phase change.

Figure 5 shows the gas sensing response curve for Sn-doped TiO_2 nanoparticles synthesized by microwave-assisted and solid-state diffusion route towards the CO_2

gas. Response curves clearly show the good dependence on concentration of CO_2 gas. As the concentration of CO_2 gas increases, resistance of the sensor also increases. This may be due to the oxidizing nature of CO_2 gas. The sensing curves for both samples are almost linear up to 300 ppm, but beyond that diverted from linearity. This may be a CO_2 detection limit for as-synthesized samples. With view of comparison, Sn-doped TiO_2 nanoparticles synthesized by microwave-assisted route show higher response than solid-state diffusion route. This may be because microwave heating is more uniform and avoids thermal gradients present in conventional heating. In SEM analysis, it is observed that Sn-doped TiO_2 flakes are more separate than solid-state diffusion route. Therefore, sample provides larger area to test gas for adsorption. This may increase the interaction probability of gas–solid.

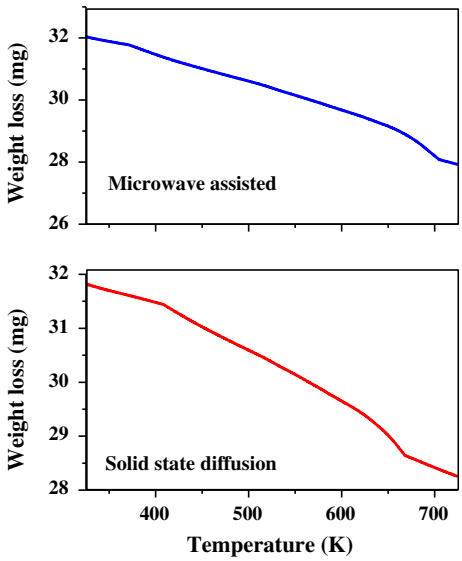

Fig. 4 TGA curves of Sn-doped TiO_2 nanoparticles synthesized by microwave-assisted and solid-state diffusion route

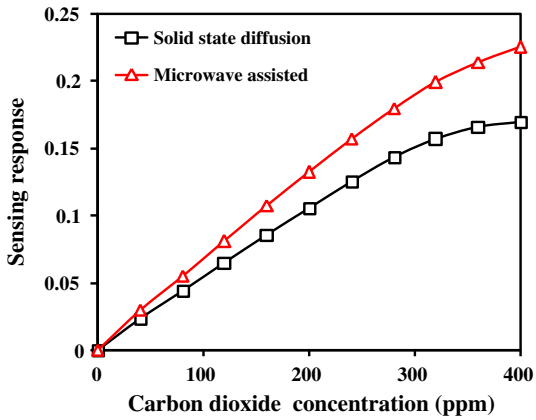

Fig. 5 Gas sensing response of Sn-doped TiO_2 nanoparticles synthesized by microwave-assisted and solid-state diffusion route

The mechanism for CO_2 gas detection for these materials is based on bridging oxygen mechanism. Reactions that occur at the sensor surface are mainly assisted by adsorbed oxygen. The change in concentration of adsorbed oxygen may alter the sensing response. Therefore, modification of pristine TiO_2 by Sn results in creating additional adsorption site and catalyzes the surface redox reaction.

We suggest that the oxygen adsorbed on the sensor surface may be involved in the sensing process of CO_2. The interface between adsorbed atmospheric oxygen and sensing surface is shown below (Fan et al. 2013).

$$O_2\,(\text{gas}) \rightarrow O_2\,(\text{ads})$$
$$O_2\,(\text{ads}) + e^- \rightarrow O_2^-\,(\text{ads})$$
$$O_2^-\,(\text{ads}) + e^- \rightarrow 2O^-\,(\text{ads})$$

Therefore, CO_2 may initially adsorb on pre-adsorbed oxygen and form surface carbonate. The plausible sensing

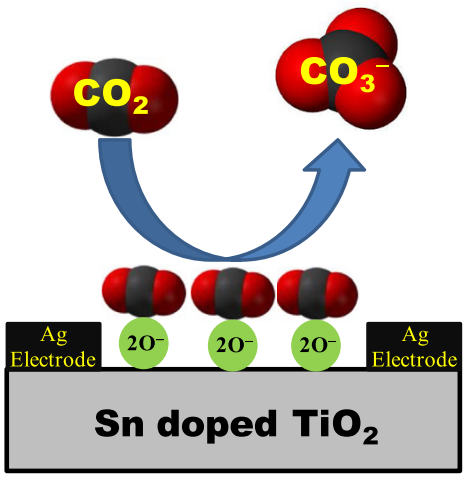

Fig. 6 Plausible sensing mechanism for CO_2 detection

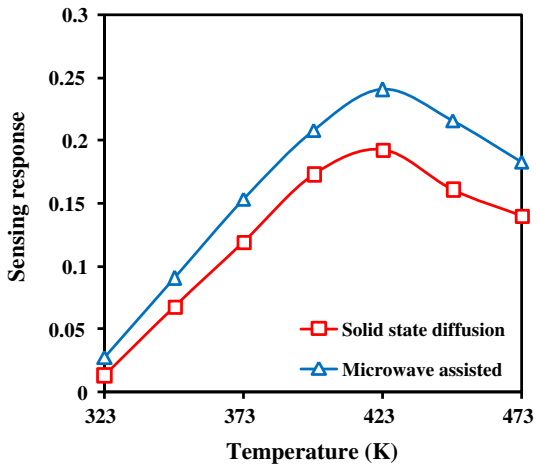

Fig. 7 Operating temperature response of Sn-doped TiO_2 nanoparticles to 200 ppm CO_2 gas

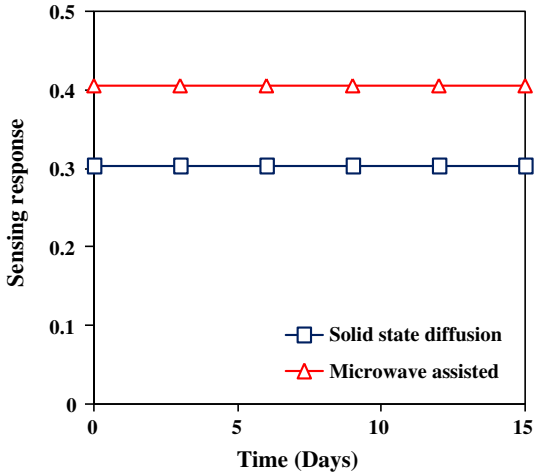

Fig. 8 Stability response of Sn-doped TiO_2 nanoparticles to 400 ppm concentration of CO_2 at 423 K

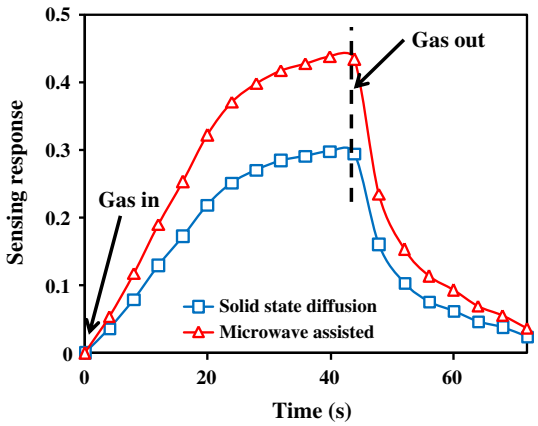

Fig. 9 Transient response of Sn-doped TiO_2 nanoparticles to 400 ppm concentration of CO_2 at 423 K

mechanism for CO_2 detection is represented as Fig. 6. This formation of surface carbonates was responsible for the CO_2 detection through resistance change.

Figure 7 shows the operating temperature characteristics of as-synthesized materials for 30 ppm CO_2 gas. In the measured temperature domain, response to 200 ppm CO_2 increases up to 423 K and finally drops. This decrease in response value may be due to desorption of atmospheric oxygen ions from sensing surface due to thermal vibrations (Nemade and Waghuley 2013). Therefore, highest value of the sensing response at 423 K may be considered as operating temperature of Sn-doped TiO_2 gas sensing materials.

Figure 8 shows stability characteristics of as-synthesized Sn-doped TiO_2 nanoparticles for 400 ppm concentration of CO_2 at 423 K. To check the stability of sensor, its response was measured for 15 days, at an interval of 3 days. Both the sensors have almost constant sensing response. This shows that stability of both sensors is good against CO_2.

The transient response characteristic of Sn-doped TiO_2 nanoparticles based on both sensors for 400 ppm CO_2 at 423 K was studied and is shown in Fig. 9. For this measurement, gas was introduced in the chamber and resistance of sensors was measured in background gas, that is air and in the presence of CO_2 gas. Both sensors show fast response time towards the CO_2 of the order 42 s. For measuring the recovery time, sensors were exposed to air. Both the sensors achieve fast recovery in 30 s.

Conclusions

We have comparatively demonstrated CO_2 gas sensing by Sn-doped TiO_2 nanoparticles, which were synthesized by microwave-assisted and solid-state diffusion route. The structural analysis by XRD, pointed out the formation samples. The Sn-doped TiO_2 nanoparticles synthesized by microwave-assisted route found to be efficient for the good sensing response of CO_2 gas, due to sufficient sensing response at room temperature and relatively low operating temperature. The sensors realized the detection of CO_2 with fast response and recovery. Both the sensors were found to exhibit good stability against CO_2.

Acknowledgments One of the authors, K.R. Nemade is very much thankful to Shri Sanjayji Agrawal, Chairman, Jaidev Education Society and Shri Ajayji Agrawal, Secretary, Jaidev Education Society for providing necessary facilities.

References

Al-Homoudi I, Thakur JS, Naik R, Auner GW, Newaz G (2007) Anatase TiO_2 films based CO gas sensor: film thickness, substrate and temperature effects. Appl Surf Sci 253:8607–8614

Benkara S, Zerkouta S, Ghamrid H (2013) Synthesis of Sn doped ZnO/TiO_2 nanocomposite film and their application to H_2 gas sensing properties. Mater Sci Semi Process 16:1271–1279

Choi HG, Yong S, Kim DK (2012) Synthesis and photocatalytic properties of SnO_2-mixed and Sn-doped TiO_2 nanoparticles. Kor J Mater Res 22:352–357

Duan Y, Fu N, Liu Q, Fang Y, Zhou X, Zhang J, Lin Y (2012) Sn-doped TiO_2 photoanode for dye-sensitized solar cells. J Phys Chem C 116:8888–8893

Fan K, Qin H, Wang L, Ju L, Hu J (2013) CO_2 gas sensors based on $La_{1-x}Sr_xFeO_3$ nanocrystalline powders. Sens Actuators B 177:265–269

Lopez IA, Vazquez A, Gomez I (2013) Microwave assisted synthesis of CdS nanoparticles and their size evolution. Rev Mex Fis 59:160–164

Nemade KR, Waghuley SA (2013a) Chemiresistive gas sensing by few-layered graphene. J Electro Mater 42:2857–2866

Nemade KR, Waghuley SA (2013b) Strontium oxide quantum dot decorated graphene composites for liquid petroleum gas sensing. J Chinese Adv Mater Soc 1:219–228

Nemade KR, Waghuley SA (2014a) Role of defects concentration on optical and carbon dioxide gas sensing properties of Sb_2O_3/graphene composites. Optical Mater 36:712–716

Nemade KR, Waghuley SA (2014b) Low temperature synthesis of semiconducting α-Al_2O_3 quantum dots. Ceram Int 40:6109–6113

Radecka M, Jasinski M, Klich-Kafel J, Rekas M, Lyson B, Czapla A, Lubecka M, Sokolowski M, Zakrzewska K, Heel A, Graule TJ (2010) TiO_2-based nanopowders for gas sensor. Ceram Mater 62:545–549

Raji P, Binitha HS, Kumar KB (2011) Synthesis and humidity sensing properties of Sn-doped nano- TiO_2. J Nanotechnol 2011:569036–569042

Sui R, Young JL, Berlinguette CP (2010) Sol–gel synthesis of linear Sn-doped TiO_2 nanostructures. J Mater Chem 20:498–503

Sun B, Shi T, Peng Z, Sheng W, Jiang T, Liao G (2013) Controlled fabrication of Sn/TiO_2 nanorods for photoelectrochemical water splitting. Nanoscale Res Lett 8:462–470

Surati MA, Jauhari S, Desai KR (2012) A brief review: microwave assisted organic reaction. Arch Appl Sci Res 4:645–661

Wu JM (2012) Tin-doped rutile titanium dioxide nanowires: luminescence, gas sensor, and field emission properties. J Nanosci Nanotechnol 12:1434–1439

Xiufeng Z, Juan L, Lianghai L, Zuoshan W (2011) Preparation of crystalline Sn-doped TiO_2 and its application in visible-light photocatalysis. J Nanomater 2011:432947–432952